

Does Gravitational Clustering Stabilize On Small Scales?

Bhuvnesh Jain

Max-Planck-Institut für Astrophysik, Karl-Schwarzschild-Strasse 1, 85740 Garching, Germany

Email: bjain@mpa-garching.mpg.de

ABSTRACT

The stable clustering hypothesis is a key analytical anchor on the nonlinear dynamics of gravitational clustering in cosmology. It states that on sufficiently small scales the mean pair velocity approaches zero, or equivalently, that the mean number of neighbours of a particle remains constant in time at a given physical separation. N-body simulations have only recently achieved sufficient resolution to probe the regime of correlation function amplitudes $\xi \sim 100 - 10^4$ in which stable clustering might be valid. In this paper we use N-body simulations of scale free spectra $P(k) \propto k^n$ with $-2 \leq n \leq 0$ and of the CDM spectrum to apply two tests for stable clustering: the time evolution and shape of $\xi(x, t)$, and the mean pair velocity on small scales. We solve the pair conservation equation to measure the mean pair velocity, as it provides a more accurate estimate from the simulation data. For all spectra the results are consistent with the stable clustering predictions on the smallest scales probed, $x < 0.07 x_{nl}(t)$, where $x_{nl}(t)$ is the correlation length. The measured stable clustering regime corresponds to a typical range of $200 \lesssim \xi \lesssim 2000$, though spectra with more small scale power ($n \simeq 0$) approach the stable clustering asymptote at larger values of ξ .

We test the amplitude of ξ predicted by the analytical model of Sheth & Jain (1996), and find agreement to within 20% in the stable clustering regime for nearly all spectra. For the CDM spectrum the nonlinear ξ is accurately approximated by this model with $n \simeq -2$ on physical scales $\lesssim 100 - 300 h^{-1} \text{kpc}$ for $\sigma_8 = 0.5 - 1$, and on smaller scales at earlier times. The growth of ξ for CDM-like models is discussed in the context of a power law parameterization often used to describe galaxy clustering at high redshifts. The growth parameter ϵ is computed as a function of time and length scale, and found to be larger than 1 in the moderately nonlinear regime – thus the growth of ξ is much faster on scales of interest than is commonly assumed.

Key words: galaxies: clustering-cosmology: theory-dark matter

1 INTRODUCTION

The stable clustering hypothesis is one of the few analytical handles on the deeply nonlinear regime of gravitational clustering. It states that the mean relative velocity of particle pairs in physical coordinates is zero. Hence in comoving coordinates the mean relative velocity exactly cancels the Hubble recession velocity between pairs of particles. As we will see below, this is equivalent to the statement that the mean number of neighbours of a particle in physical coordinates remains constant in time. The stable clustering hypothesis invokes the physical picture of a virialized cluster which has separated out from the expanding background, and is neither expanding nor contracting. Since on small scales, any statistical measure is dominated by the contribution from dense clusters, the clustering should statistically be stable.

This hypothesis leads to predictions for the evolution in time of the autocorrelation function ξ . In the case of scale free spectra which display self-similar scaling, the slope of $\xi(x)$ in the small scale regime is predicted as well. For $\xi \gg 1$ it is extremely difficult to make analytical approximations to the growth of clustering. Hence the stable clustering hypothesis has been very useful in relating the shape of ξ and the power spectrum $P(k)$ in the nonlinear regime to the initial spectrum. Peebles (1974) and Gott & Rees (1975) implemented the first such applications. The widely used property of hierarchical scaling of the higher order moments of the density in terms of its second moment also derives from the dynamics of stable clustering. As emphasized in the next section, this property requires additional assumptions of stability at each order in the distribution.

N-body simulations are the ideal tool to test stable clus-

tering. Efstathiou et al. (1988) carried out a pioneering study of self-similar evolution, and tested the small scale ξ and v for stable clustering. Their data were consistent with the stable clustering slope for ξ on the smallest scales, but their 32^3 particle simulations lacked the resolution to give any definitive conclusion. Recently Padmanabhan et al. (1995) and Colombi, Bouchet & Hernquist (1995; hereafter CBH), have tested the stable clustering predictions for ξ , v , and in the latter case for the hierarchical form of the higher moments S_3 , S_4 and S_5 as well. While Padmanabhan et al. (1995) found departures from stable clustering in their $\Omega = 1$ simulations, CBH verified the stable clustering prediction in their tests of ξ . However, they found small departures from the hierarchical relation for the higher moments.

In this paper we use P³M (particle-particle/particle-mesh) simulations with $100^3 - 144^3$ particles to test stable clustering for power law spectra with $-2 \leq n \leq 0$, and for the CDM spectrum. We measure ξ and v , for which we use the pair conservation equation to obtain estimates with greater accuracy than allowed by direct measurements. Our approach and numerical resolution is similar to that of CBH, with the advantage that we have 4 – 10 times as many particles. We do not however test for the higher moments as they do. While stable clustering predicts the slope of ξ , its amplitude can be approximated by additional assumptions as done in the analytical model of Sheth & Jain (1996). We test their predictions against the measured amplitude in the N-body data. We also test for stable clustering in two high resolution CDM simulations and identify the range of scales and epochs on which it is an adequate approximation.

We begin in the next section with the relevant BBGKY equations through which the stable clustering hypothesis leads to the predictions for ξ and the higher moments. In Section 3 we outline a secondary infall model which can be connected with the nonlinear form of ξ , and discuss the dynamical effects which might invalidate stable clustering. Section 4 contains a description of the N-body simulations, and an analysis of the effects of limited numerical resolution on small scales. Section 5 presents the main results for ξ , with the mean pair velocity results in Section 5.1, and results for the CDM spectrum in Section 5.2. We conclude in Section 6.

2 THE BBGKY HIERARCHY EQUATIONS

The stable clustering hypothesis yields the form of the nonlinear correlation function when applied to the moments of the BBGKY hierarchy equations. The presentation below follows that of Peebles (1980, Sections 71 and 73).

The second equation of the BBGKY hierarchy of equations, when integrated over momenta, yields the pair conservation equation. This equation connects the rate of change of the autocorrelation function $\xi(x, t)$ to the mean pair velocity in comoving coordinates, $v(x, t) = a\dot{x}$:

$$\frac{\partial \xi}{\partial t} + \frac{1}{x^2 a} \frac{\partial}{\partial x} [x^2 (1 + \xi) v] = 0. \quad (1)$$

Integrating the above equation over a sphere of radius x gives

$$\frac{\partial}{\partial t} \left[na^3 4\pi \int_0^x dx' x'^2 (1 + \xi) \right] + 4\pi a^2 x^2 n (1 + \xi) v = 0, \quad (2)$$

where $n(t) \propto a^{-3}$ is the number density in physical coordinates. From the definition of ξ it follows that $n(t) a^3 4\pi x^2 dx [1 + \xi(x, t)]$ is the typical number of neighbours in a spherical shell of thickness dx at a distance x from a particle. Thus the first term in equation (2) is the rate of change of neighbours inside a sphere of radius x , while the second term is the flux of particles through the surface of the sphere – hence the name pair conservation equation.

The stable clustering hypothesis is the statement that the relative pair velocity in comoving coordinates, $a\dot{x}$, exactly cancels the Hubble velocity, $\dot{a}x$, so that the mean pair velocity in physical coordinates $d(ax)/dt = 0$. On substituting this assumption,

$$v(x, t) = -\dot{a}x, \quad (3)$$

in (1), the functional form of $\xi(x, t)$ which satisfies the equation becomes restricted to

$$1 + \xi = a^3 f[a(t)x], \quad (4)$$

and we can approximate $1 + \xi \simeq \xi$, as the stable clustering hypothesis is applied on very small scales where ξ is at least of order 100. Equation (4) thus fixes the growth of ξ in physical coordinates: $\xi(r, t) \propto a^3$. Physically it means that the typical number of neighbors per unit volume, at small enough separations r from a particle, remains constant in time, as it is $\simeq n(t)\xi(r, t)$, and $n(t) \propto a^{-3}$ as noted above.

If the universe is spatially flat, with $\Omega = \Omega_{matter} = 1$, and the initial spectrum of perturbations is a pure power law $P(k) \propto k^n$, the subsequent evolution is expected to be self-similar (Peebles 1980, Section 73). Then $\xi(x, t)$ and $P(k, t)$ take the special functional form:

$$\xi(x, t) = \hat{\xi}(x/x_0 a^\alpha); \quad P(k, t) = a^{3\alpha} k_0^{-3} \hat{P}(ka^\alpha/k_0), \quad (5)$$

where $\alpha = 2/(3 + n)$; k_0, x_0 are constants which must be determined from the initial conditions; and $\hat{P}, \hat{\xi}$ are unspecified dimensionless functions. It is easy to verify that the linear spectrum $P_1(k, t) \propto a^2 k^n$ is consistent with the functional form of equation (5). The linear mean squared density contrast on length scale k^{-1} scales as $a^2 k^{-(3+n)}$, hence equating it to unity gives the same scaling, $k \propto a^{-2/(3+n)}$ as contained in equation (5). This unique scaling in time of characteristic length scales is the essence of self-similar evolution.

Equating the functional forms of ξ given by equations (4) and (5) restricts the t and x dependence of ξ to be a pure power law. The solution for ξ , and similarly for P , is:

$$\xi(x, t) \propto (x/a^\alpha)^{-\gamma}; \quad P(k, t) \propto a^{\frac{6}{(5+n)}} k^{\frac{-6}{(5+n)}}, \quad (6)$$

where $\gamma = (9 + 3n)/(5 + n)$. Thus the stable clustering assumption, in conjunction with the requirement of self-similarity, fixes both the asymptotic growth and the shape of the power spectrum/correlation function. While self-similarity is an idealization as it requires the initial spectrum to be a pure power law, it can be a useful approximation to a more realistic description, and as we shall see it is very useful for testing the dynamical validity of stable clustering.

For completeness we re-write the pair conservation equation (2) in terms of the mean interior correlation function, which is the integral of the correlation function over a sphere, divided by the volume of the sphere:

$$\bar{\xi}(x, t) \equiv \frac{3}{x^3} \int_0^x dx x^2 \xi(x, t). \quad (7)$$

Using this definition and re-arranging terms in equation (2) gives

$$\frac{a}{3(1+\xi)} \frac{\partial \bar{\xi}}{\partial a} = \frac{-v}{\dot{a}x} \equiv \frac{-v}{Hr}, \quad (8)$$

where Hr is the Hubble velocity on the physical scale $r = ax$. In Section 4 we shall use this form of the pair conservation equation to measure the mean pair velocity v from the N-body simulations.

2.1 Hierarchical relation of higher moments

The hierarchical form of the 3-point function $\zeta_{123} \equiv \zeta(r_{12}, r_{23}, r_{31})$ and of the higher moments can also be related to the stability assumption. Here we outline the argument which motivates the hierarchical form using self-similarity and stable clustering. The purpose of this exercise is to point out that additional assumptions of stability at every order in the particle distribution are needed to obtain the hierarchical form at that order. These go beyond the assumption $-v/Hr = 1$ used to obtain the stable clustering shape of ξ .

Following Peebles (1980), consider the equation of conservation of triplets of particles, obtained by integrating over momenta the 3rd equation of the BBGKY hierarchy. In terms of the relative velocities of particle pairs, it can be written as

$$a \frac{\partial h_3}{\partial t} + \frac{\partial}{\partial \vec{x}_{12}} \cdot \vec{w}_{12} h_3 + \frac{\partial}{\partial \vec{x}_{31}} \cdot \vec{w}_{31} h_3 = 0, \quad (9)$$

where $h_3 = 1 + \xi_{12} + \xi_{23} + \xi_{31} + \zeta_{123}$, and \vec{w}_{ij} is the mean pair velocity of particles i, j given the position of the third particle in the triangle formed by the triplet. This definition makes \vec{w}_{12} a different statistic from \vec{v}_{12} : the former is a 3-point statistic as it is obtained by integrating over momenta the 3-point distribution function, while the latter is a 2-point statistic.

In equation (9) if we assume that $w_{12} = -\dot{a}x_{12}$ and $w_{31} = -\dot{a}x_{31}$ on small scales, then we are led to the functional form $h_3 \equiv a^6 h(ax_{12}, ax_{23})$. Combined with the constraint of self-similarity this leads to a power law solution for h_3 and therefore for the three point function: $\zeta \propto x^{-2\gamma}$, where x is the size of the triangle, and γ is the stable clustering slope of ξ defined following equation (6). It is thus consistent with the form

$$\zeta_{123} = Q(\xi_{12}\xi_{23} + \xi_{23}\xi_{31} + \xi_{31}\xi_{12}), \quad (10)$$

which is the widely used hierarchical form for the 3-point function. This argument can be generalized to the 4- and 5-point functions, and has been found to agree with results of N-body simulations as well as observations of galaxies.

The argument leading to the hierarchical form for ζ makes an assumption about the 3-point particle distribution. Likewise for the N -th order correlation function, the assumption required is that the mean relative velocity of particle pairs, given the presence of $N - 2$ other particles, be zero. Therefore additional conditions of stability are needed at each order of the hierarchy to get the analogues of equation (10) for higher order moments. These conditions clearly go beyond the assumption $v = -\dot{a}x$ which led to equation (6) for the second moment ξ . The tests performed in this

paper relate to ξ , and therefore do not necessarily verify the assumptions leading to the hierarchical form of higher moments. This is also relevant in comparing our results with those of CBH, who appear to find small departures from the hierarchical relation for the S_3, S_4 and S_5 parameters (while their results for ξ are consistent with ours as discussed in Section 5).

3 ANALYTICAL MODELS

For convenience in modelling, small scale clustering can be thought of in two somewhat distinct ways. One is the hierarchical growth of structure by the continuous mergers of smaller clumps. N-body simulations have highlighted the importance of mergers, but the detailed dynamics is very difficult to model analytically. The other model, known as secondary infall, visualizes a more gradual and spherically symmetric accretion of matter on to initial density peaks leading to the formation of a halo. Simulations show that spherically symmetric accretion rarely occurs in the formation of typical halos. But one might imagine that the average properties of halos are well approximated by the outcome of such a secondary infall model.

The advantage of the secondary infall picture is that it is analytically tractable, and the density profile of a halo resulting from a given initial profile can be calculated. Gunn & Gott (1972) and Gott (1975) made the first calculations of spherical accretion models, while Fillmore & Goldreich (1984) and Bertschinger (1985) obtained detailed solutions for the profile arising from the late time behavior of particle orbits. Hoffman & Shaham's (1987) influential paper applied these results to the structure of halos formed in a cosmological setting. The secondary infall solution for the density profile can also be connected to the nonlinear form of ξ (Padmanabhan et al. 1995; Padmanabhan 1996; Sheth & Jain 1996). Here we outline this connection, and comment on its implications for the validity of stable clustering. This section is a bit of a detour from the main body of the paper, and some readers may wish to skip to sub-section 3.2 which provides a summary of the section.

Consider a spherically symmetric distribution of collisionless particles with an initial density profile

$$\frac{\delta\rho}{\rho}(x, t_i) \propto x^{-\kappa}. \quad (11)$$

Note that κ here is 3ϵ in the notation of Fillmore and Goldreich (1984) as they used the mass as the variable on the RHS. Let these particles be assigned velocities such that they are in Hubble flow at some initial time t_i . The trajectories of these particles will follow radial orbits, and since they are in overdense regions, they will eventually stop expanding and collapse towards the center of mass. The point at which particles with an initial radius x_i first stop expanding is known as turnaround, and the turnaround radius denoted $x_{ta}(x_i)$ depends on x_i . After turnaround, since the particles are taken to be collisionless, they execute oscillations about the center of mass.

Fillmore & Goldreich obtained self-similar solutions for the final distribution of these particles by using the adiabatic invariance of the mass $M(x, t)$ within a given radius x . Consider the orbit of a particle with maximum radius much

smaller than the current turnaround radius. By assuming $M(x, t)$ to vary sufficiently slowly that it could be treated as a constant over the timescale of oscillation of this particle, they solved for the variation in time of the maximum radius of the particle in terms of its turnaround radius. This in turn allowed them to obtain the asymptotic (late time) density profile in terms of the initial density profile. The result is:

$$\frac{\delta\rho}{\rho}(x, t_{\text{asym}}) \propto x^{\frac{-3\kappa}{(1+\kappa)}} \quad ; \quad \kappa \geq 2. \quad (12)$$

The shape of the final density profile in the secondary infall model is qualitatively different if $\kappa < 2$, i.e. if the initial density profile is sufficiently shallow. The dynamical origin of this difference is that for $\kappa < 2$, at late times the mass within a radius x is dominated by the contribution from particles with maximum radii $> x$. In contrast, for $\kappa > 2$, the mass within x is dominated by particles with maximum radii $< x$. The consequence of this difference is that for $\kappa < 2$, particle orbits on small scales keep shrinking due to the increasing mass contributed by large scales. The late time density profile approaches a form that does not depend on the initial profile. The asymptotic density profile is given by

$$\frac{\delta\rho}{\rho}(x, t_{\text{asym}}) \propto x^{-2} \quad ; \quad \kappa < 2. \quad (13)$$

The above discussion relies on purely radial orbits. The sharp transition at $\kappa = 2$ does not occur if one allows the particles to have some angular momentum. White and Zaritsky (1992) have studied the density profiles arising from an initial distribution of angular momentum in which the eccentricity is constant as a function of radius. In such a case, the transition to a regime of x^{-2} density profiles does not occur at all, and the form of equation (12) is always valid. More generally one might find that a finite angular momentum causes the density profiles to lie somewhere in between the shapes of equation (12) and (13) for $\kappa < 2$, and to maintain the shape of equation (12) for $\kappa \geq 2$.

3.1 From secondary infall to stable clustering

We are now in a position to apply the secondary infall model to the autocorrelation function ξ in an Einstein-de Sitter cosmology. The hope is that what works for an isolated halo also applies statistically to the full matter distribution with an appropriate matching of initial profiles. Consider the ingredients that led to the stable clustering profile of equation (6). (i) The pair conservation equation, which is simply a kinematical expression of the conservation of particle number. (ii) Self-similarity, namely that characteristic length scales grow as a power law of time: $x \propto a(t)^{2/(3+n)}$. (iii) Expanding coordinates, implicit in the use of the comoving spatial coordinate \vec{x} .

Each of these ingredients is present in the secondary infall model described above. Thus stable clustering relies on such a limited aspect of the dynamics of the full distribution, that the model of an isolated spherically symmetric object can satisfy the conditions under which it is applied. To connect the two models, we need to relate the initial density profile of the secondary infall model to the initial spectrum of the cosmological distribution. Unfortunately there is no rigorous way to make this connection. We show below that

the stable clustering slope for ξ is recovered if the initial density profile is taken proportional to the rms smoothed density fluctuation of the cosmological distribution (Padmanabhan et al. 1995) which is given by

$$\frac{\delta\rho}{\rho}(x, t_i) \propto x^{-\kappa} \propto x^{-(3+n)/2}. \quad (14)$$

The Fillmore-Goldreich result for the final profile given by equations (12) and (13) can now be directly adapted, with the substitution $\kappa = (3+n)/2$. Thus the transition value of $\kappa = 2$ corresponds to $n = 1$, and the asymptotic shape of ξ is

$$\xi(x, t_{\text{asym}}) \propto x^{-\frac{(9+3n)}{(5+n)}} \quad ; \quad n \geq 1, \quad (15)$$

corresponding to equation (12), and,

$$\xi(x, t_{\text{asym}}) \propto x^{-2} \quad ; \quad n < 1, \quad (16)$$

corresponding to equation (13).

Equation (15) shows one way to connect the stable clustering profile to the nonlinear density profile of an isolated spherical halo. Since the choice of the initial profile was made in hindsight, in order to recover the desired shape of ξ , this is not intended to be a “derivation” of stable clustering. What it does in fact demonstrate is that there could be a regime in which stable clustering is *invalid*. With the particular initial profile chosen here, stable clustering holds only if the initial spectral index $n > 1$ – a range of very little interest for realistic spectra like the CDM spectrum, since for all scales of interest n ranges between 1 and -3 (or lower for spectra with some hot-dark matter). Taken at face value this result suggests that for spectra of interest stable clustering is invalid, and that the nonlinear ξ should take the universal shape $\xi \propto x^{-2}$, independent of the initial spectrum.

However, as discussed above, the presence of nonradial orbits lowers the transition value of κ and of n , and possibly completely eliminates the regime of an x^{-2} profile. The key parameter therefore becomes the degree of eccentricity of the orbits – if the eccentricity stays roughly constant, or increases with the size of the orbit, then infalling particles will not contribute to the mass inside a given x and orbits will not asymptotically shrink. In such a case, the profile will retain the stable clustering prediction of equation (15).

One can also consider a more detailed model in which pairs with small separation x are taken to belong to stable halos, so that $\xi(x)$ arises from the convolution of the density profiles of such halos (Sheth & Jain 1996). The stable clustering shape of ξ can be obtained from the secondary infall result with an appropriate initial halo profile, but again there is no rigorous justification for this initial profile.

3.2 Summary

The lesson from the secondary infall models for ξ is that they show how the stability assumption can be invalidated in cases where the initial profile is sufficiently shallow. The key dynamical factor is the distribution of angular momentum. Particles with large orbital radii need to have sufficient angular momentum, else their contribution to the mass inside arbitrarily small radii causes small scale orbits to asymptotically shrink. This corresponds to a net infall pair velocity, and could lead to a universal x^{-2} shape for ξ , independent of the initial n for spectra of interest.

In the formation of halos a more important process appears to be the hierarchical merging of smaller halos. The influence of merging on small scale dynamics can depend critically on the size of halos which contribute most of the pairs at small separations. If most of the pairs with separation x belong to the cores of halos of radii much larger than x , then ongoing mergers of roughly equal mass halos might cause the cores to expand and lead to a net outflow pair velocity. On the other hand if members of pairs come from halos with radii of order, or smaller than, x , then the merging of such halos could lead to net infall pair velocities. These considerations highlight some mechanisms which could violate the stability assumption, and cause ξ to become either steeper or shallower than the stable clustering shape. But the limitations of analytical modelling leave N-body simulations as the only realistic means of testing for stable clustering.

4 N-BODY SIMULATIONS

This section provides some details of the N-body simulations used to obtain the results presented in the next section. Six different simulations are analyzed in this paper. Two are for the standard CDM spectrum. The other four are for power-law spectra with $n = 0, -1, -1.5$ and -2 with $\Omega = 1$. All the simulations were performed using high resolution P³M codes. Table 1 shows some important parameters for the different simulations: the total number of particles N_{part} , the Plummer force softening parameter ϵ , the size of the PM mesh, and the smallest comoving scale x_{min} on which ξ can be reliably measured.

For models with $-1.5 \leq n \leq 0$, the simulations used were performed by S. White, with the same code as in EFWD. The total number of particles is 100^3 and the force resolution equivalent to a Plummer softening parameter $\epsilon = L/2500$, where L is the size of the computational box. The $n = -2$ run was performed by E. Bertschinger using an adaptive P³M code. It followed 128^3 particles with $\epsilon = L/2560$. The CDM simulation denoted CDM1 in Table 1, is the same as in Gelb & Bertschinger (1994). It is a P³M simulation with 144^3 particles, $\Omega = 1$, $H_0 = 50$ km/s/Mpc, $L = 100$ Mpc and $\epsilon = 65$ kpc. It is normalized so that σ_8 (the linear rms mass fluctuation in a sphere of radius 16Mpc) is unity when the expansion factor $a = 1$. For CDM at early times, $a < 0.5$, we have used the results of a smaller box simulation performed by S. White. This simulation, denoted CDM2, has 100^3 particles in a 50 Mpc box, with a force resolution equivalent to $\epsilon = 20$ kpc.

4.1 Numerical Resolution Effects

In using N-body simulations to study gravitational clustering, there are several numerical artifacts that need to be carefully eliminated. In this sub-section, we focus on those effects that are most relevant in studying the small-scale dynamics of interest for this work. There are two critical factors: (i) The suppression of ξ on small scales due to force softening and 2-body relaxation, and, (ii) Effects due to the initial conditions and the finite volume of the simulation box which limit the range of time outputs and length scales over which clustering follows the true dynamics. We provide

estimates of the relevant numerical effects, and thus arrive at criteria for the range of scales on which the statistical measures used are reliable. For the scale free spectra these criteria are verified by testing for self-similar scaling.

A comprehensive study and tests of numerical effects can be found in CBH, Baugh et al. (1995) and Gelb (1992). These authors have tested the effects of finite resolution, discreteness, and statistical fluctuations in the initial conditions on different statistical measures. Their results on small scales and on 2-point statistics are relevant here, as the simulations used by them are of comparable resolution to those used in this study. Tormen et al. (1996) have made detailed tests of numerical resolution in the context of measuring density profiles of halos – these are also relevant as ξ is closely related to the halo profiles.

Initial conditions. At early times the particle distribution is affected by the cubical grid from which the particles are perturbed, and by transients due to the Zel'dovich approximation used to set up the initial perturbations. The effect of the grid can be minimized by starting with “glass” initial conditions, as has been done in the simulations for $-1.5 \leq n \leq 0$ (see White 1994 for a discussion of “glass” initial conditions). In general, to ensure that there are no artifacts due to the initial conditions, the initial amplitude of the perturbations should be chosen small. A test for how small is sufficient is provided by checking for self-similarity, since the evolution of scale free initial spectra is expected to be self-similar once it follows the true dynamics. The initial amplitude used in the scale free simulations with $-1.5 \leq n \leq 0$ is such that the power on the Nyquist frequency of the particle grid equals the white noise level (Efsthathiou et al. 1988). For $n = -2$, as noted by Lacey & Cole (1994), departures from self-similarity persist for rather late times. Hence the initial amplitude needs to be lower for $n = -2$; it was chosen such that the dimensionless power on the Nyquist frequency of the particle grid is $4\pi k^3 P(k) = 0.03$.

Force softening. To suppress the effects of two-body relaxation, force softening is implemented in computing short range forces in the particle-particle part of the simulations by using the equivalent of a Plummer force law: $F(r) = Gm^2r/(r^2 + \epsilon^2)^{3/2}$. The parameter ϵ is given in Table 1 for the different simulations used. The results shown in Figure 1 for $\xi(a, x)$ extend to 2ϵ on the small scale end. As compared to the exact Newtonian force Gm^2/r^2 , the fractional error in $F(r)$ at $r = 2\epsilon$ is 28%. The results in Figure 1 show that for the first one or two points plotted, in the range $2\epsilon < x < 3 - 4\epsilon$, ξ is underestimated, especially at earlier times. As discussed below, the cause for the artificial suppression of ξ at earlier times is usually due to 2-body relaxation and not force softening.

Discreteness effects: 2-body relaxation. The effect of force softening is easy to quantify, as described above, and since ϵ is constant in comoving coordinates, it is expected to affect the same range of scales at all times. But the distribution at separations $> 2\epsilon$ may still be inaccurate if randomly chosen particles do not have enough neighbours within such a separation, due to the effects of 2-body relaxation. A simple estimate can be made because $1 + \xi(x)$, when integrated over a sphere of radius x , is the mean number of neighbours within separation x from a randomly chosen particle. For ξ

Table 1. Parameters of the N-body simulations

Simulation	N_{part}	Softening ϵ/L	PM Mesh	x_{min}/ϵ
$n = 0$	100^3	1/2500	256^3	2 – 4
$n = -1$	100^3	1/2500	256^3	2 – 4
$n = -1.5$	100^3	1/2500	256^3	2.5 – 5
$n = -2$	128^3	1/2560	$256^3 - 432^3$	3 – 5
CDM1	144^3	65Kpc/100Mpc	$288^3 - 420^3$	2 – 3
CDM2	100^3	20Kpc/50Mpc	256^3	3 – 4

large enough this is essentially the total number of neighbours. Therefore with $x = m\epsilon \simeq mL/2000$, where m is of order 2 – 5, and $N_{part}^3/L^3 \simeq 10^6/L^3$ being the mean number density, we can estimate the mean number of neighbours to be:

$$N_{nbrs} = \frac{4\pi}{3-\gamma} \left(\frac{N_{total}}{10^6} \right) \left(\frac{\xi}{10^3} \right) \left(\frac{m}{2} \right)^3. \quad (17)$$

In obtaining the above equation, we have assumed that $\xi \propto x^{-\gamma}$ down to $x = 0$, with $\gamma = 1 - 1.8$ for the spectra of interest. In the simulations however, ξ is suppressed on very small scales. The extreme case is given by setting $\gamma = 0$ which decreases N_{nbrs} by a factor of $\simeq 2$.

We use the empirical criterion that $N_{nbrs} > 10$ is required to measure ξ accurately. The resulting minimum scale x_{min} is given in Table 1 and is $> 2\epsilon$ at the two earlier time outputs shown in Figure 1 (in stars and circles). It is typically smaller than 2ϵ for the last output, in which case we set $x_{min} = 2\epsilon$ due to the effect of force softening. Taking the minimum reliable scale to be the larger of the values that satisfy the criteria of accurate forces and sufficient particle number successfully identifies the small scale regime in which the measured ξ departs from self-similarity. For CDM we have checked that the measured ξ in the two simulations, which have different values of N_{nbrs} at a given scale, are in very good agreement on the scales used in our analysis (see Figure 4). Our results for x_{min} are similar to those of CBH after adjusting for the different particle number and force softening.

Range of $x_{nl}(a)$. At late times the nonlinear scale $x_{nl}(a)$, defined by equation (18), approaches the size of the box. This sets a maximum value of a beyond which the clustering is artificially suppressed due to the absence of modes with wavelength larger than the box-size. This problem is particularly severe for spectra with $n \leq -2$ because they have more power on large scales relative to spectra with higher n , which in turns leads to a stronger nonlinear coupling with small scale modes. It is the principal reason for the difficulty in obtaining self-similar scaling for the $n = -2$ spectrum. For spectra with $n > -2$ we find that $x_{nl}(a) > L/10$ is sufficient to obtain accurate self-similar scaling on the scales of interest. This is the criterion used to set the maximum time output for our analysis.

At very early times there are transient effects from the initial conditions, and moreover clustering on small scales has not fully developed. We allow for an expansion factor of at least 4, and in the case of $n = -2$ of 12, between the initial time and the first output used for our analysis. At this time the nonlinear scale is in the range $x_{nl} \simeq L/50 - L/100$.

Other effects.

PM mesh: The mesh used to compute the long range forces in the PM (particle-mesh) part of the force computation also introduces an artificial scale. But if the particle-particle forces are computed for a conservatively chosen set of particles at each timestep, as is done for the simulations used here, then the effects of the mesh are virtually absent (Bertschinger 1991).

Poisson fluctuations: To compute ξ at a given radius, sums over particles within logarithmically spaced radial bins are made. Poisson fluctuations within each radial bin produces errors in the measured ξ . This effect is also negligible as the number of pairs measured is large enough that the resulting fluctuations in ξ are smaller than 1%, and would appear smaller than the symbols shown in Figures 1 and 2.

Finite volume effects: At low wavenumbers the finite number of modes present in a given bin in k causes statistical fluctuations in the initial power spectrum. As nonlinear evolution proceeds, these low- k modes couple to the modes at higher k and can in principle lead to fluctuations in the distribution at small scales as well. Also, modes with wavelength larger than the box-size are absent. In practice for the range of $x_{nl}(a)$ used, there is negligible effect on scales smaller than $L/10$, which is the range of scales of interest here. The effect is not negligible on the higher moments of the density, as emphasized by CBH and Baugh et al. But for the evolution of ξ the fluctuations between different realizations are about 2 – 3% on the small scales. We have checked this by comparing ξ for simulations started from three different realizations of the $n = -1$ spectrum.

5 RESULTS

Self-similarity provides a powerful simplification in studying the evolution of scale-free spectra in an Einstein-de Sitter universe. Using the self-similar solution for $\xi(a, x)$ from equation (6), we define a characteristic nonlinear scale $x_{nl}(a)$ as

$$\xi(a, x_{nl}) \equiv 1 \quad ; \quad x_{nl}(a) \propto a^{2/(3+n)}. \quad (18)$$

In the results presented in this section, the comoving distance x will be scaled by $x_{nl}(a)$ at each time. Expressed as a function of $x/x_{nl}(a)$ the correlation function ξ , or any dimensionless statistic, is independent of time if the evolution is self-similar. This allows the measured correlation function at different times to be combined so that the effective dynamic range of the simulation is extended. See Jain & Bertschinger (1996) for an analytical analysis, and CBH and

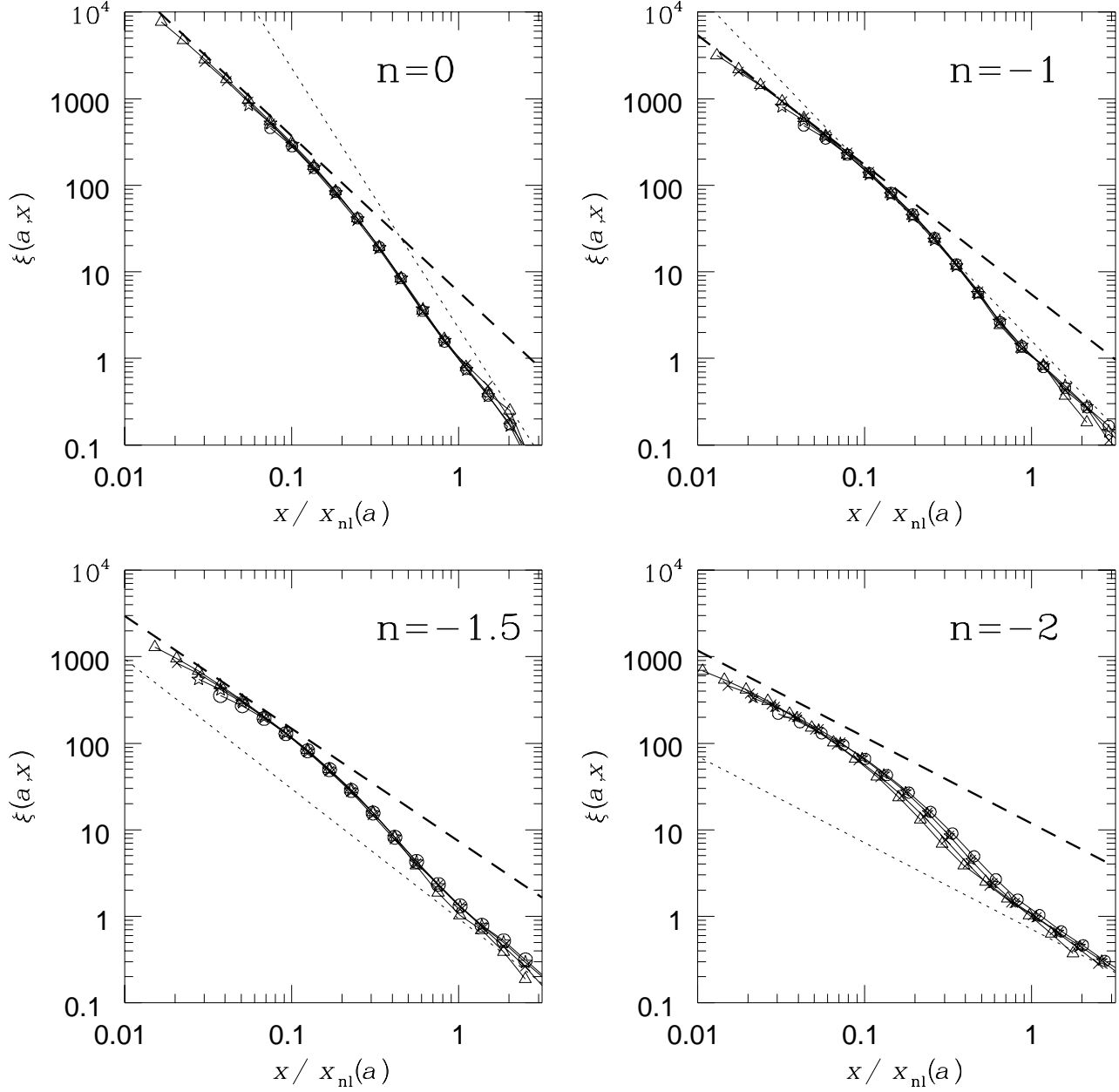


Figure 1. Self-similarly scaled correlation functions. Each panel shows $\xi(a, x)$ computed at four time outputs from simulations of scale free spectra with $n = 0, -1, -1.5, -2$ as indicated in the panels. It is plotted against $x/x_{nl}(a)$, where $\xi(a, x_{nl}) = 1$ defines the nonlinear scale $x_{nl}(a)$ at each $a(t)$. Between successive time outputs $x_{nl}(a)$ grows by a factor of $\simeq 1.5$. The circles, stars, crosses and triangles show the outputs at successively later times, and therefore at later stages of nonlinearity. The dotted line is the linear ξ . The dashed line shows the stable clustering slope for ξ ; its amplitude is given by the model of Sheth & Jain (equations 19 and 20).

Padmanabhan et al. (1995) for numerical tests of self-similar evolution.

Figure 1 shows $\xi(x/x_{nl}(a))$ for four different power law spectra. In each panel four output times are used to compute ξ . The figure shows that self-similar scaling is convincingly verified for all the spectra, with the possible exception of the $n = -2$ case which shows some scatter. Small departures from self-similarity can be seen at the smallest and largest scales. On small scales the departures arise because ξ is underestimated due to the effects of force softening and finite particle number. The effect is very small for all points except for the very last, which corresponds to a separation $\simeq 2\epsilon$. On large scales the correlation function is affected, especially at late times, by the absence of waves that are larger than the size of the box. This causes ξ at late times to fall below the self-similar curve.

As pointed out by CBH, a simple way to estimate the self-similar ξ for a given spectrum, is to take the largest of the different values measured at different times for each value of $x/x_{nl}(a)$. This should give a reasonable result for the cases where there is some scatter, as in $n = -2$, or the small scale end of all the spectra. The rationale is that numerical limitations cause a suppression of ξ , both at small and large scales. However, we shall not need to do this because for the scales of interest, the measured ξ are sufficiently self-similar without any corrections.

With the self-similarly scaled correlation functions for different spectra, the prediction of stable clustering can be tested. The dashed lines in each of the panels of Figure 1 show the slope predicted by stable clustering. It is evident that on the smallest scales, for about a factor of 5 in $x/x_{nl}(a)$, the measured slope of ξ agrees with the stable clustering slope. As a first approximation this occurs for $\xi \gg 100$ for all spectra. A more detailed examination of the slope of ξ in Figure 1 and of the mean pair velocity in Figure 3 shows that the onset of stable clustering occurs at higher ξ for spectra with larger n ; thus for $n = -1.5$ stable clustering is valid for $\xi \gtrsim 200$, whereas for $n = 0$, it is valid for $\xi \gtrsim 500$.

Interestingly, the amplitudes of ξ which demarcate the onset of stable clustering correspond to approximately the same value of x/x_{nl} independent of the initial spectrum: $x/x_{nl}(a) \lesssim 0.07$. This provides a convenient demarcation of the stable clustering regime as it is independent of the spectrum or of any feature of self-similarity, and can therefore be applied to realistic spectra like the CDM spectrum. The variation with n in the value of ξ corresponding to $x/x_{nl}(a) \lesssim 0.07$ arises because spectra with larger n have steeper ξ in the regime of $0.07 < x/x_{nl} < 1$. Since $\xi(x_{nl}) = 1$ by definition, $\xi(0.07x_{nl})$ increases with n .

The amplitude of the stable clustering ξ , i.e. the normalization of the dashed line in Figure 1, has been fixed by the analytical model of Sheth & Jain (1996). Their calculation assumed that on small scales ξ is determined by the density profiles of collapsed halos. They fixed the shape of the profile by assuming the validity of stable clustering, and used the Press-Schechter form for the number density of halos to then predict the amplitude of ξ . The final result, equation (16) of Sheth & Jain, can be re-written as

$$\xi(x/x_{nl}) = C_n \left(\frac{x}{x_{nl}} \right)^{-\gamma}, \quad (19)$$

where $\gamma = 3(3+n)/(5+n)$ is the stable clustering slope, and C_n is an n -dependent constant. For the spectra used in this paper it takes the values,

$$\begin{aligned} C_n &= \{5.93, 5.40, 7.42, 11.96\} & \text{for} \\ n &= \{0, -1, -1.5, -2\}, \end{aligned} \quad (20)$$

respectively.

The results show that again, except possibly for $n = -2$, the measured ξ is in remarkably good agreement with the predicted value. For the range of small scales with $\xi > 200$, the measured ξ for $-1.5 \leq n \leq 0$ is within $\simeq 10\%$ of the prediction. For $n = -2$ the predicted value is larger by $\simeq 30\%$ for the maximum measured ξ . For this case, the large scatter between the different time outputs suggests that even the maximum measured ξ at a given x/x_{nl} is an underestimate of the true value; the dashed line might therefore be accurate at the same level as the other cases. The verification of the amplitude of ξ predicted by equation (19) implies that both stable clustering and the Press-Schechter model provide accurate descriptions of nonlinear clustering for a wide range of spectra. It also suggests that it is reasonable to assume that ξ is determined by the structure of dark halos on sufficiently small scales. The trend that the onset of stable clustering occurs for larger values of ξ as n increases is also in agreement with the estimate of Sheth & Jain, which assumed that only the half-mass radii of virialized halos have stabilized. Our results can be used to estimate the free parameter in the spherical model for ξ used by Padmanabhan et al. (1995). The choice $m = 3$ in their equation (14) gives closest agreement with our results.

5.1 Mean pair velocity

The stable clustering hypothesis can also be tested by directly computing the mean relative velocity of pairs of particle. In physical coordinates this velocity should approach zero as the pair separation is made vanishingly small. In comoving coordinates therefore, the mean pair velocity $v(a, x) = a\dot{x}$ must exactly cancel the Hubble velocity $Hr = \dot{a}x$, so that the ratio $-a\dot{x}/Hr = 1$.

However $v(a, x)$ is much more noisy than $\xi(a, x)$, because of the high dispersion in the pair velocity. This is illustrated in Figure 2 where the measured $-v/Hr$ is plotted against $\bar{\xi}$ for $n = -1$. It is only on averaging the data from three realizations that a meaningful result is obtained. At least five realizations for each spectrum would be needed to directly measure $-v/Hr$ to better than 20%. In the absence of such extensive simulation data, we use an indirect method to measure $-v/Hr$.

As described in Section 2, the evolution of ξ is connected with v via the pair conservation equation. Therefore to the extent that the simulation is accurate, v can be measured using the evolution of ξ , and should give the same result as would be obtained from a simulation with enough particles to reduce the noise in the directly measured v . We use the form of the pair conservation equation given in equation (8) to solve for v . We evaluate the time derivative of $\bar{\xi}$ by taking logarithmic derivatives. Since the evolution of ξ and $\bar{\xi}$ is close to a power law in a , taking logarithmic derivatives reduces the error introduced by the finite time interval be-

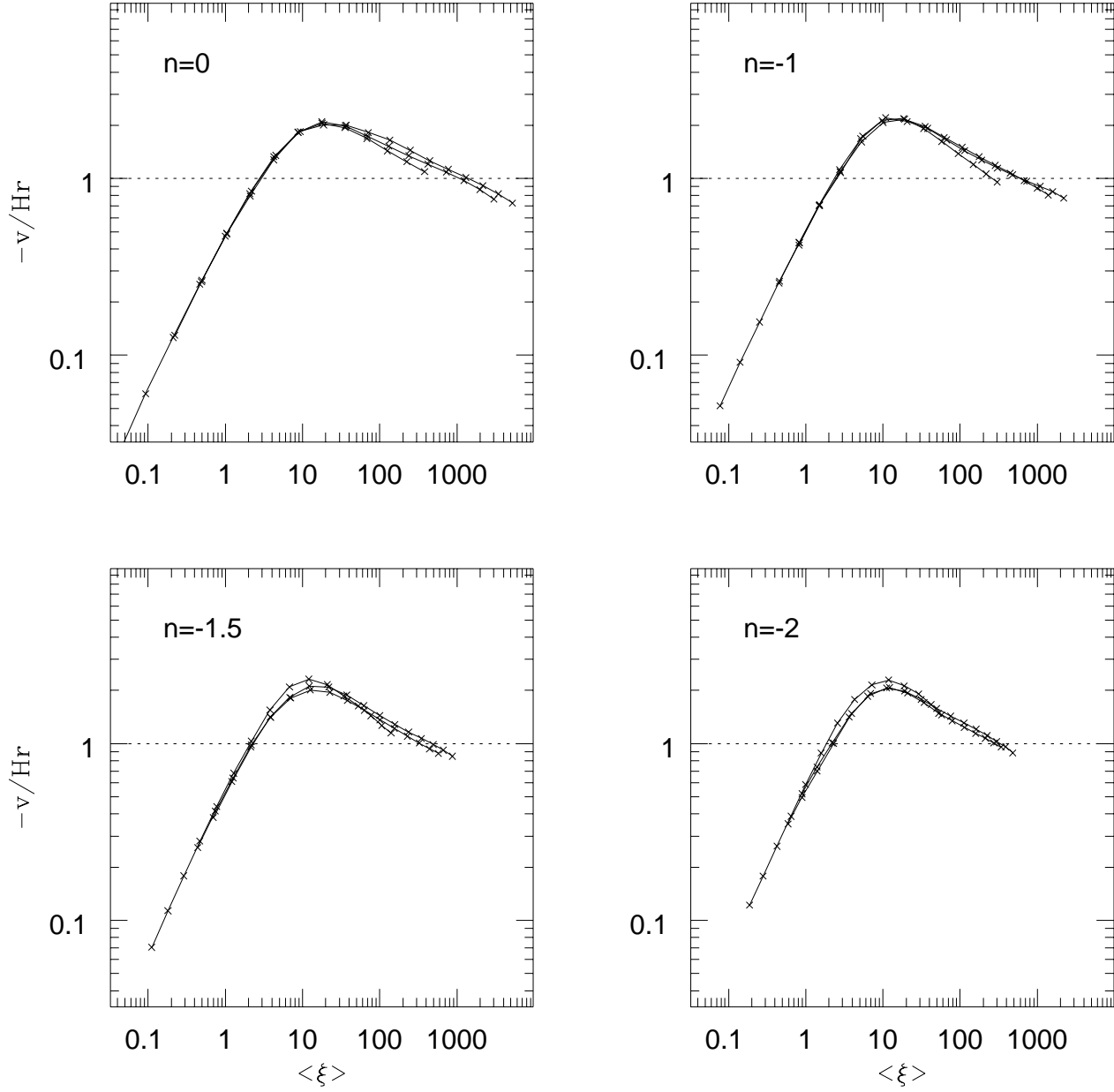


Figure 3. The ratio of the mean pair (peculiar) velocity to the Hubble velocity, $-v/Hr$, as a function of the mean correlation function $\bar{\xi}$. The pair conservation equation is used to solve for $-v/Hr$ using the evolution of $\bar{\xi}(a, x)$, as discussed in the text. Results are shown for three output times, corresponding approximately to the outputs shown in Figure 1, for the same set of scale free spectra. The near coincidence of the curves at different times verifies self-similarity, while the approach to the dotted line $-v/Hr = 1$ is consistent with stable clustering.

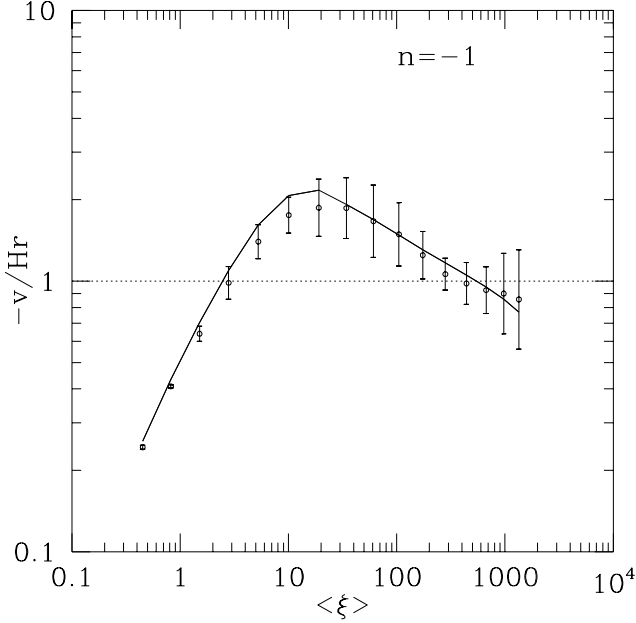


Figure 2. Mean pair velocity for $n = -1$. Simulations of three different realizations of the $n = -1$ spectrum are used to directly measure $-v/Hr$. The average value is shown by the circular data points, with the error bars showing the $1\text{-}\sigma$ deviations of the distribution. The solid curve shows $-v/Hr$ computed using the pair conservation equation as in Figure 3, for the same output time as the circular points.

tween successive outputs. To estimate $-v/Hr$ for a given x at output time a_i we use the finite difference equation

$$\frac{-v}{Hr}(a_i) = \frac{\bar{\xi}(a_i)}{3[1 + \bar{\xi}(a_i)]} \left[\frac{\log \bar{\xi}(a_{i+1}) - \log \bar{\xi}(a_{i-1})}{\log a_{i+1} - \log a_{i-1}} \right]. \quad (21)$$

While the mean pair velocity contains the same information as the evolution of ξ , it tests for stable clustering more directly for generic spectra like CDM which do not evolve self-similarly.

The results for the inferred $-v/Hr$ are shown in Figure 3 for three time outputs of the scale free spectra with $n = 0, -1, -1.5, -2$. Self-similarity requires that the data at different time outputs coincide, since both $-v/Hr$ and $\bar{\xi}$ are dimensionless functions of $x/x_{nl}(a)$. On scales with $\bar{\xi} < 1$ the linear theory relation $-v/Hr \propto \bar{\xi}$ is verified. For larger values of $\bar{\xi}$, the ratio $-v/Hr$ turns over after reaching a maximum value of $\simeq 2$ at $\bar{\xi} \simeq 10$. For $\bar{\xi} > 100$, the ratio approaches unity, though it appears to continue to decline with increasing $\bar{\xi}$ for a given time. For the range of $\bar{\xi}$ for which the slope in Figure 1 agrees with the stable clustering value, the measured $-v/Hr = 1$ to within about 20% for almost all the data. While this is a satisfactory consistency check, $-v/Hr$ does not appear to flatten into an asymptotic regime up to the highest $\bar{\xi}$ measured.

The results for $-v/Hr$ on small scales are less reliable than the results for ξ because the former depends directly on $\bar{\xi}(x)$, which is an integral of ξ over scales smaller than x , and is therefore suppressed even for $x > x_{min}$. This artificial suppression largely accounts for the continued decline in the

measured curves below the line $-v/Hr = 1$. We verified that if $\xi(x < \epsilon)$ is fixed at the stable clustering slope, then on scales in the range $2\epsilon < x < 4\epsilon$, shown by the last 3 points at each time output, $-v/Hr$ would indeed be almost flat. Larger simulations, which accurately measure $-v/Hr$ on scales significantly smaller than in our simulations, are needed to test its approach to the line $-v/Hr = 1$.

While the evidence for the existence of an asymptotic regime in Figure 1 for ξ is still weak, the results for ξ and the mean pair velocity are certainly consistent with stable clustering on the smallest scales probed. These results are in agreement with those of CBH, who used tree-code simulations in their analysis, with force resolution comparable to our simulations and $< 1/4$ the number of particles. Padmanabhan et al. (1995) however concluded that for $\Omega = 1$, stable clustering is violated as they obtained $-v/Hr > 1$. A careful comparison of their results with ours reveals that the results from their P³M simulations are consistent with ours, and with stable clustering. But the results for $n = -2$ and $n = -1$ from their PM simulations are inconsistent with ours at the maximum $\bar{\xi}$ measured in their simulations (typically a factor of 2–3 smaller than ours). The reasons for this discrepancy are not clear, and merit a detailed comparison of clustering in high-density regions in PM and P³M simulations.

5.2 Evolution of the CDM spectrum

The results for ξ and v for the standard CDM spectrum with $\sigma_8 = 1$ at $a = 1$ are shown in Figures 4–8. Figure 4 shows ξ measured at 4 different redshifts in the range $0.2 < a < 1$. We use results from both simulations to maximize the range of scales on which ξ can be accurately measured. At early times, for $a < 0.5$, when the correlation length $x_{nl} < 5$ Mpc, we measure ξ from the simulation with a smaller box-size, CDM2, as it has better resolution on small scales. For $a > 0.5$ CDM1 is used as x_{nl} becomes larger than $L/10$ for CDM2. We are thus able to measure ξ down to $x_{nl}/30$ for $a = 0.2$, and $x_{nl}/100$ for $a > 0.4$. Since the results of Figure 1 show that $x/x_{nl} < 0.07$ is required for stable clustering, we have a sufficient range of x to test the CDM model in the range $0.2 < a < 1$.

Unlike the scale free spectra, for CDM it is not possible to scale self-similarly and compare ξ at different times. However, if stable clustering is valid, then expressed as a function of the separation $r = ax$ in physical coordinates, $\xi(a, r)$ must grow in time as a^3 (see equation (4)) so that the mean number of neighbours $\propto a^{-3}\xi(a, r)$ remains constant. We therefore test for the constancy of $a^{-3}\xi(a, r)$ on sufficiently small scales in the two panels of Figure 5 for four values of the expansion factor in each panel. Since the onset of stable clustering should occur approximately at a fixed value of ξ , the physical scale at which this occurs increases with a . Figure 6 shows the evolution of the correlation length $r_{nl}(a)$ with a . The values of $r = 0.07 r_{nl}(a)$ for the four values of a in each panel of Figure 5 are shown by the circles at the bottom. Thus for the curve extending to the smallest r , the onset of stable clustering is marked by the left-most circle. The values of $r = 0.07 r_{nl}(a)$ are 20, 180, 700 kpc for $a = 0.2, 0.5, 1$ respectively. The rapid growth of $r_{nl}(a)$ makes it difficult to assess for stability for non-power law spectra by comparing ξ at different times. But within the region of

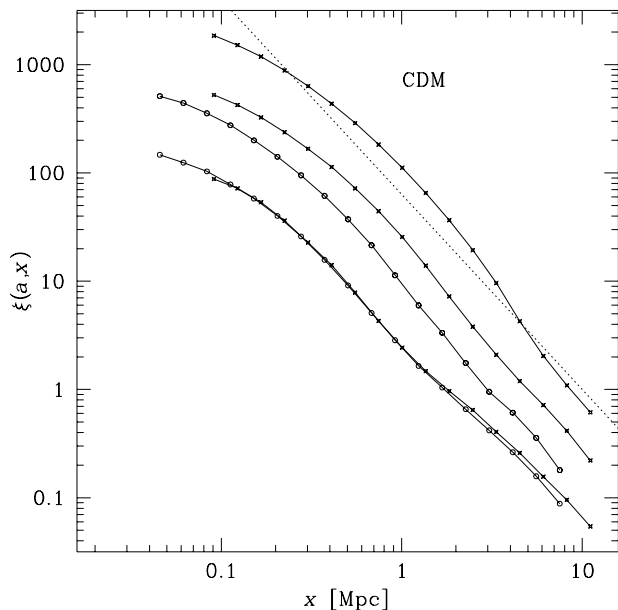


Figure 4. Correlation function for the CDM spectrum. The solid curves show $\xi(a, x)$ computed from two simulations of the standard Cold Dark Matter power spectrum at four output times, with $a = 0.21, 0.32, 0.51, 1.0$. The data shown in circles are from a simulation with a box size $L = 50$ Mpc, and those in stars are from a bigger box with $L = 100$ Mpc. To check for the accuracy of the measured ξ , the data at $a = 0.2$ from both simulations are shown. The dotted line shows the observed galaxy auto-correlation function with slope $= -1.8$.

overlap to the left of the circles, the different curves are very close to each other. The results are therefore consistent with stable clustering, as verified also by the plot of $-v/Hr$ in Figure 8.

Both the amplitude and slope of ξ on small scales are very well approximated by the dashed line in Figure 5, which is the same as for the $n = -2$ spectrum in Figure 1. Thus its slope is -1 and its amplitude is set by equations (19) and (20) with $n = -2$. For the lower panel in Figure 5, with $a < 0.5$, the measured slope of ξ is shallower, as it is sensitive to the part of the CDM spectrum with $n < -2$. However the $n = -2$ line is still an adequate approximation. We conclude that for CDM-like spectra the slope and amplitude of ξ on small scales is not very sensitive to the precise shape of the spectrum, and is approximated rather well by the stable clustering result for a power law spectrum with $n \simeq -2$.

Finally we test a parameterization of the evolution of ξ commonly used in studies of clustering of galaxies and Lyman-alpha clouds at high redshift. The correlation function is taken to have the form:

$$\xi(a, r) = a^{3+\epsilon} \left(\frac{r}{r_0} \right)^{-\gamma_0}, \quad (22)$$

where $\gamma_0 = 1.8$ is the observed slope of the galaxy correlation function, and $r_0 \simeq 5h^{-1}\text{Mpc}$ is the correlation length at $a = 1$. The parameter $\epsilon = 0$ in the stable clustering regime and 0.8 in the linear regime. Our results show that there are two main reasons why such a parameterization is

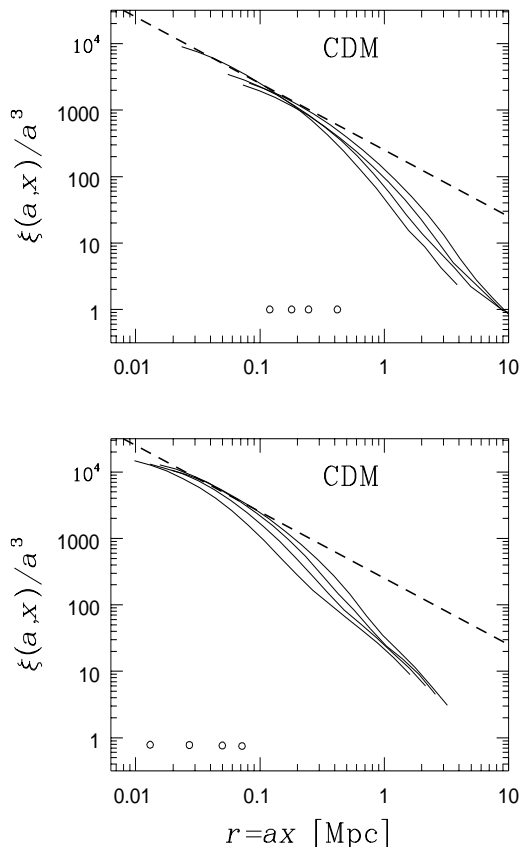


Figure 5. Scaled correlation function for the CDM spectrum. The two panels show $\xi(a, x)/a^3$ for the CDM spectrum plotted against the physical length scale $r = ax$. The different curves should coincide in the stable clustering regime. The upper panel shows expansion factors $a = 0.51, 0.60, 0.81, 1.0$, and the lower panel shows $a = 0.21, 0.28, 0.34, 0.43$. The data for $a > 0.5$ and $a < 0.5$ are separated as the numerical resolution limit on small scales precludes their comparison over a common range in r in the stable clustering regime. The slope and amplitude of the dashed lines in both panels are the same as the stable clustering values for $n = -2$ shown in Figure 1. The x-coordinate of the circles marked towards the bottom is the scale $0.07 r_{nl}(a)$; for given a stable clustering is expected for $r < 0.07 r_{nl}(a)$ as discussed in the text.

inaccurate in the context of any CDM-like model. First, the growth of $\xi(a, r)$ in the intermediate regime is much faster than a^3 , so the stable clustering and linear regime do not give the upper and lower bound for the growth rate of ξ . Second, the onset of the stable clustering regime, and of the intermediate regime as well, occurs on a scale which grows rapidly with a . Therefore to parameterize the shape of ξ by one or two power laws which remain fixed in time is not accurate. For general use, following Hamilton et al. (1991) and Nityananda & Padmanabhan (1994), universal fitting formulae have been proposed for the nonlinear ξ which apply to any smooth initial spectrum (see Jain, Mo & White 1995 and Peacock & Dodds 1996).

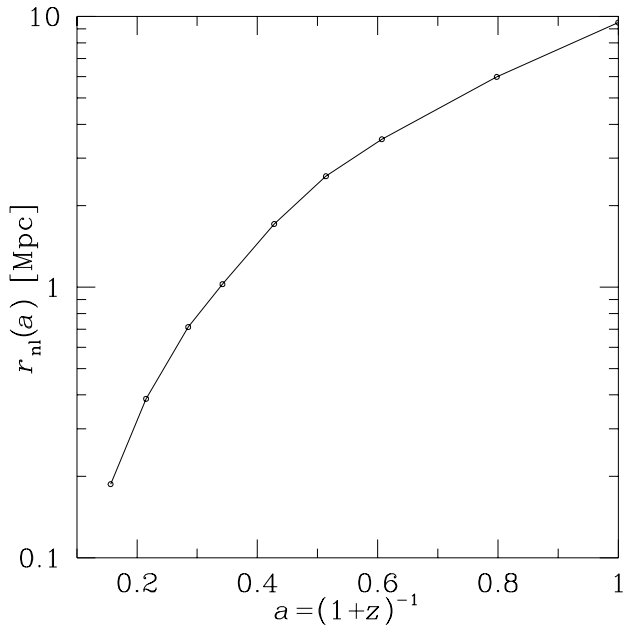


Figure 6. Correlation length for the CDM spectrum. The measured correlation length in physical coordinates, defined by $\xi(a, r_{nl}) = 1$, for the CDM spectrum is shown for $0.15 < a < 1$. The scale $0.07 r_{nl}(a)$, shown in Figure 5 to mark the onset of stable clustering, can be read off from this plot for a given a .

However, if for reasons of convenience, a parameterization like that of equation (22) is used, the results of Figures 5 and 7 show that $\epsilon = 0$ is a good approximation for $r/r_{nl} < 0.07$, with $r_{nl}(a)$ shown in Figure 6. In the regime $0.07 < r/r_{nl} < 1$ the growth rate varies rapidly, rising to $\epsilon \simeq 2$ before approaching the linear theory value $\epsilon = 0.8$ at $r \simeq r_{nl}$. Thus in the intermediate regime between the stable clustering and linear regimes, ϵ is typically larger than 1, and is significantly underestimated if it is taken to be 0.

Figures 6 and 7 can be used to estimate ϵ for a CDM-like model in which the growth of ξ is parameterized as: $\xi(a, r) = a^{3+\epsilon} \tilde{\xi}(r)$, with $\tilde{\xi}$ being a function only of r in some narrow range of a . Figure 6 gives $r_{nl}(a)$ for any desired $a = 1/(1+z)$, and Figure 7 can then be used to read off ϵ at the range of physical separations r of interest. For CDM-like spectra and with $\Omega = 1$, the results of Figure 7 are not sensitive to the shape of the spectrum and to the choice of a in the range $0.2 \lesssim a \lesssim 1$. This discussion is of course subject to the uncertainties due to the possible biasing of galaxies relative to the dark matter.

6 DISCUSSION

The results presented in this paper can be summarized as follows.

- The shape and evolution of the correlation function $\xi(a, x)$ is consistent with the stable clustering prediction of equation (6). We have verified this result with the power spectrum measured from the simulations presented here as well.
- Direct measurement of the mean pair velocity is not suf-

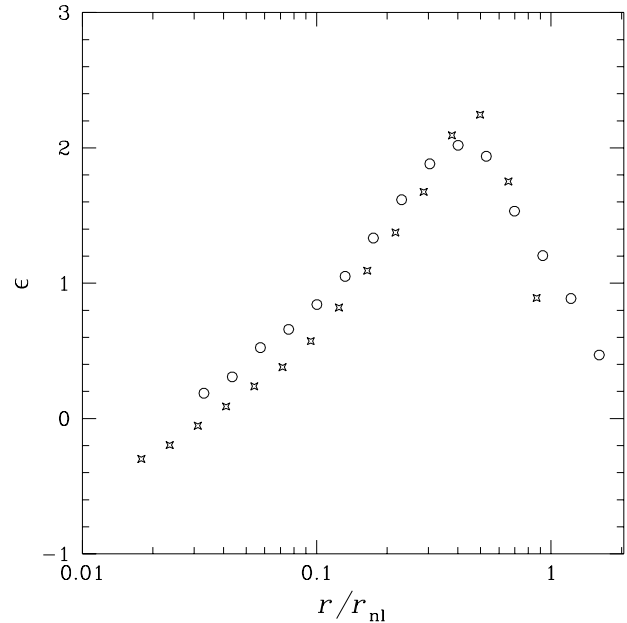


Figure 7. Growth of $\xi(a, r)$ for CDM. For a power law parameterization of the form $\xi(a, r) = a^{3+\epsilon} \tilde{\xi}(r)$, ϵ is shown as a function of r/r_{nl} . The circles and stars are for $a = 0.28$ and $a = 0.51$ respectively. The variation of ϵ with r/r_{nl} shows that a simple power law form for all r is not accurate, and that in the regime $0.1 < r/r_{nl} < 1$, the growth rate is much faster than the commonly used values of $\epsilon = 0$ or 0.8 . The value of ϵ can be obtained as a function of r for any desired $a = 1/(1+z)$ by using Figure 6 to get $r_{nl}(a)$.

ficiently accurate on small scales. We have therefore solved the pair conservation equation to estimate $-v/Hr$ which approaches unity on small scales, as required for consistency with the results for ξ .

- We find that the onset of stable clustering occurs at $x/x_{nl}(a) = 0.07$ for all spectra tested. This provides a useful way to demarcate the stable clustering regime for generic spectra. The range of ξ over which stable clustering is verified is typically $200 < \xi < 2000$; it is higher for initial spectra with more small scale power ($n \simeq 0$).

- For the CDM spectrum we find the range of scales for $0.2 < a < 1$ for which the evolution of ξ is consistent with stable clustering. The combination of simulations with two different box-sizes enabled us to study clustering on very small scales, typically down to comoving scales = 40 – 120 kpc (with $h = 0.5$), while retaining the nonlinear influence of sufficiently long waves on the dynamics. The physical scale demarcating the stable clustering regime rapidly increases with time, and is about $r = 20, 180, 700$ kpc for $a = 0.2, 0.5, 1$ respectively.

- The amplitude of the nonlinear ξ agrees to better than 20% with the prediction of the Press-Schechter model of Sheth & Jain (1996) for nearly all the spectra studied. For the CDM spectrum the results agree with the predicted slope and amplitude of the $n = -2$ spectrum. The agreement of the model for different initial spectra is remarkable in view of the fact that their nonlinear behavior is quite different:

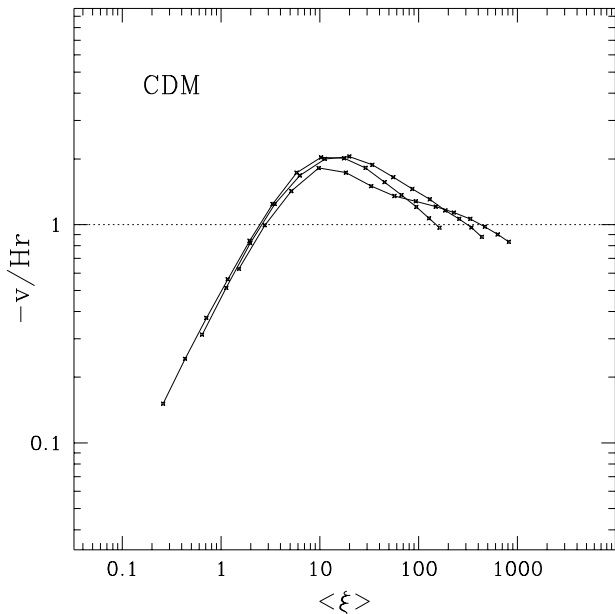


Figure 8. Mean pair velocity for the CDM spectrum. The mean pair velocity is computed using the pair conservation equation as in Figure 3. The three curves are for $a = 0.3, 0.6, 0.8$. Note that unlike Figure 3, for CDM-like spectra the curves at different times are not expected to coincide. They do however approach the stable clustering value $-v/Hr = 1$ for $\bar{\xi} > 200$.

e.g. for $n = 0$ the nonlinear ξ is suppressed relative to the linear ξ by an order of magnitude, while for $n \simeq -2$ it is enhanced by about the same factor.

• We emphasize that the commonly used parameterization $\xi = a^{3+\epsilon} (r/r_0)^{-1.8}$, with $\epsilon = 0$ is accurate only in the stable clustering regime of $r/r_{nl} < 0.07$. It can severely underestimate the growth of ξ in the intermediate regime of $0.07 < r/r_{nl} < 1$ in which the growth of ξ varies rapidly with r , ranging from $\epsilon \simeq 0 - 2$. The results shown in Figures 6 and 7 can be used to estimate ϵ for given r and a for CDM-like spectra.

For a numerical study aimed at testing an asymptotic regime it is appropriate to conclude on a note of caution. Small scale clustering is closely linked to the structure of the inner parts of dark halos. Both the number density and density profile of very small halos, with $M \ll M^*/10$, are poorly resolved in N-body simulations – this can crucially affect the shape of ξ in the small scale limit (S. White, private communication; Sheth & Jain 1996).

Thus while the simulations used in this study provide strong evidence that gravitational clustering stabilizes on scales smaller than $\sim 1/10$ th the nonlinear scale, it is premature to draw conclusions about a possible asymptotic regime. We have shown results typically over a factor of 5 in length scale, and an order of magnitude in ξ , by using self-similar scaling to combine results from different output times. The competing demands of small scale resolution and a simulation box sufficiently bigger than the non-linear scale, do not leave enough dynamic range to see a convincing asymptotic regime on small scales (say a range of scales $\gg 10$).

We have carefully analyzed the effects of limited numerical resolution to rule out the possibility of a conspiracy of numerical artifacts over the range of scales that were used in our analysis. Therefore we can conclude with confidence that any departures from stable clustering could occur only on scales with $\xi \gg 10^4$, which lie beyond our resolution limits. We shall have to wait for the next generation of high resolution simulations, with $N \gtrsim 10^8$ particles, to find possible new aspects of nonlinear clustering.

ACKNOWLEDGMENTS

I am very grateful to Ed Bertschinger and Simon White for making available their simulation data for this paper, and for stimulating discussions. I thank Martin Haehnelt, Uroš Seljak, Ravi Sheth and Bepi Tormen for helpful discussions.

REFERENCES

- Baugh C. M., Gaztanaga E., Efstathiou G. 1995, MNRAS, 274, 1049
- Bertschinger E. 1985, ApJS, 58, 39
- Bertschinger E. 1991, After the First Three Minutes, ed. S. Holt, V. Trimble & C. Bennett (New York: AIP), 297-311
- Colombi S., Bouchet F. R., Hernquist L. 1995, astro-ph/9508142 (CBH)
- Davis M., Peebles P. J. E. 1977, ApJS, 34, 425
- Efstathiou G., Frenk C. S., White S. D. M., Davis M. 1988, MNRAS, 235, 715
- Fillmore J. A., Goldreich P. 1984, ApJ, 281, 1
- Gelb J. M. 1992, PhD. Thesis, M.I.T.
- Gelb J. M., Bertschinger E., 1994, ApJ, 436, 467
- Gott III J. R. 1975, ApJ, 201, 296
- Gott III J. R., Rees M., 1975, A&A, 45, 365
- Hamilton A. J. S., Kumar P., Lu E., Matthews A. 1991, ApJL, 374, L1
- Gunn J. E., Gott III J. R. 1972, ApJ, 176, 1
- Hoffman Y., Shaham J. 1985, ApJ, 297, 16
- Jain B., Bertschinger E. 1996, ApJ, 456, 43
- Jain B., Mo H. J., White S. D. M. 1995, MNRAS, 276, L25
- Nityananda R., Padmanabhan T. 1994, MNRAS, 271, 976
- Padmanabhan T. 1995, astro-ph/9510037
- Padmanabhan T., Cen R., Ostriker J. P., Summers F.J. 1995, astro-ph/9506051
- Peacock J. A., Dodds S. J. 1996, astro-ph/9603031
- Peebles P. J. E. 1974, A&A, 181, L51
- Peebles P. J. E. 1980, The Large-Scale Structure of the Universe (Princeton: Princeton University Press)
- Sheth R., Jain B. 1996, astro-ph/9602103
- Tormen G., Bouchet F. R., White S. D. M. 1996, astro-ph/9603132
- White S. D. M. 1994, Les Houches Lectures, astro-ph/9410043
- White S. D. M., Zaritsky D. 1992, ApJ, 394, 1